



Revised cloud and convective parameterization in CFSv2 improve the underlying processes for northward propagation of Intraseasonal oscillations as proposed by the observation-based study

Malay Ganai^{1,2} · P. Mukhopadhyay¹ · R. Phani Murali Krishna^{1,3} · S. Abhik⁴ · Madhuparna Halder⁵

Received: 30 October 2018 / Accepted: 30 January 2019 / Published online: 8 February 2019
© Springer-Verlag GmbH Germany, part of Springer Nature 2019

Abstract

The performance of revised climate forecast system version 2 (CFSv2) are evaluated on the simulation of the underlying cloud and convective processes associated with the strong and weak boreal summer intraseasonal oscillations (BSISOs) events. The revised version of the CFSv2 consists of a six-class Weather Research Forecasting single moment (WSM6) cloud microphysics scheme and the default version has Zhao and Carr (ZC) cloud microphysics scheme. Both the version uses revised simplified Arakawa-Schubert (RSAS) convection scheme. The study reveals that the revised version of CFSv2 (RSAS-WSM) is able to better simulate the northward propagation of BSISOs and associated dynamical and thermodynamical mechanism put forward by earlier observation-based studies. It is found that the large-scale organized northwest-southeast tilted structure of rain band is better captured in RSAS-WSM simulation as compared to the default version of CFSv2 (RSAS-ZC) during strong BSISO events. Further, the reasonable large-scale or stratiform rainfall associated with the northward propagating strong BSISO events is seen in RSAS-WSM while it is completely missing in RSAS-ZC simulation. The pressure-latitude profiles of cloud liquid water (CLW) and cloud ice (CLI) show more realistic steady northward propagation in RSAS-WSM simulation. Consistent with the CLW and CLI distribution and their influence on the large-scale heating structure, the large-scale condensation heating shows quasi-periodic northward propagation in RSAS-WSM whereas such type of distribution is not captured in RSAS-ZC simulation. The realistic representation of cloud processes in WSM leads to simulate reasonable dynamical and thermodynamical processes associated with the strong BSISO events which follows the observation-based hypothesis proposed by earlier studies.

1 Introduction

It has been well established that the intraseasonal oscillations (ISOs) plays an important role in modulating the tropical climate (Lau and Waliser 2005; Zhang 2005). The dominant mode of tropical ISOs consists of eastward propagating convection anomaly also known as Madden–Julian

Oscillation (MJO; Madden and Julian 1971, 1994) during the boreal winter and a strong 30–60 day intraseasonal variability (ISV) characterized by pronounced northward propagation during boreal summer over the Indian subcontinent (Yasunari 1979; Sikka and Gadgil 1980; Lawrence and Webster 2002; Jiang et al. 2004). These quasi-periodic northward propagating ISVs are associated with the enhanced and suppressed phase of Indian Summer Monsoon (ISM) and contribute significantly to the ISM rainfall (Goswami 2005). Therefore, understanding the quasi-periodic northward propagating ISOs and its realistic simulation have received considerable attention of the climate community (Goswami and Xavier 2003; Webster and Hoyos 2004).

Several studies have been carried out to understand the mechanism of northward propagation of monsoon ISOs (MISOs). Webster (1983) proposed the role of sensible heat flux from planetary boundary layer (PBL) responsible for the northward propagation of convection center. Other studies by Wang and Xie (1997), Lawrence and Webster (2002)

✉ P. Mukhopadhyay
mpartha@tropmet.res.in; parthasarathi64@gmail.com

¹ Indian Institute of Tropical Meteorology (IITM), Dr. Homi Bhabha Road, Pashan, Pune 411008, India

² Savitribai Phule Pune University, Pune, India

³ Center for Prototype Climate Modeling, New York University Abu Dhabi, Abu Dhabi, United Arab Emirates

⁴ Climate Research Section, Bureau of Meteorology, Melbourne, Australia

⁵ Allahabad University, Allahabad 211002, India

documented that the northward propagation of summer ISOs resulting from Rossby wave response of the eastward propagating equatorial Kelvin-Rossby wave packets. The aspect of air-sea interaction mechanism in the northward propagation of MISO has been proposed by Kemball-Cook and Wang (2001), Fu et al. (2003), Yang et al. 2008; Sharmila et al. 2013. Based on the atmospheric general circulation model (AGCM) and reanalyses data sets, Jiang et al. (2004) provided a theoretical explanation for the northward propagation of summer ISOs. They proposed that a combination of the easterly vertical wind shear and moist convective feedback mechanism play an important role for the northward propagation of boreal summer ISOs (BSISOs). They also showed that equivalent barotropic vorticity anomaly and enhanced specific humidity in the lower troposphere are found to be shifted few degrees north of the convection center which in turn helps in preconditioning the lower atmosphere for the northward propagation of convection. Similar features have been shown by other studies based on observation (Hsu et al. 2004; Fu et al. 2006). Wang et al. (2005) showed based on high resolution satellite data that the monsoon ISOs emerge from the western equatorial Indian Ocean (EIO) and are a type of self-sustaining systems.

In spite of significant efforts to understand the BSISOs, most of the current GCMs suffer to simulate realistic BSISOs (Sperber et al. 2000; Waliser et al. 2003; Lin et al. 2008). Fu et al. (2006) attributed to the lack of understanding and proper representation of moist processes as the major source of uncertainty in the weather and climate models. Although several studies have been carried out to understand the role of different cloud regimes associated with MJO (Jakob and Tselioudis 2003; Rossow et al. 2005; Chen and Del Genio 2009; Tromeur and Rossow 2010), similar studies associated with the northward propagating BSISOs are rather limited (Xavier et al. 2007; Jiang et al. 2011, Wong et al. 2011; Halder et al. 2012; Abhik et al. 2013 (hereafter AS13)). Based on 3 years of CloudSat satellite observations and ERA-interim reanalyses data sets, Jiang et al. (2011) concluded that the shallow cumulus cloud in the lower atmosphere leads deep convection and plays a vital role in shifting northward movement of the deep convection associated with the BSISOs. By using 11 years of satellite based rainfall and cloud hydrometeors data sets, Halder et al. (2012) showed the role of different types of cloud hydrometeors associated with the northward propagation of BSISOs. They have noted that the cloud liquid water at the lower tropospheric level leads the convection center while the cloud ice slightly lags the convection centre. Apart from the above studies, AS13 utilizing satellite and reanalyses data put forward a hypothesis for northward propagation of BSISOs. They argued that realistic representation of vertical distributions of cloud hydrometeors play a key role in modulating the vertical distribution of heating which in

turn drives the upper level divergence and lower level convergence in the atmosphere. The northward propagation of rainfall anomalies associated with BSISOs were shown to be in phase with cloud liquid water while the cloud ice lags, in agreement with the findings of Jiang et al. (2011).

Recently, Abhik et al. (2017) has incorporated a six-class Weather Research Forecasting (WRF) single moment (WSM6) explicit cloud microphysical scheme (Hong and Lim 2006) in National Centre for Environmental Prediction (NCEP) climate forecast system version 2, (CFSv2) in addition to cumulus parameterization scheme, the revised SAS (Han and Pan 2011; Ganai et al. 2015, 2016). They have noted considerable improvement in the convective and large-scale precipitation distribution, northward propagation and the northwest-southeast tilt in the rainfall band during ISM. Improved representations of the sub-grid scale convection along with the grid scale cloud microphysics are attributed for better simulation of feedback between convective processes and the large-scale circulation in the model. This version of CFSv2 with WSM6 (Abhik et al. 2017) having the ability of prognosing different cloud hydrometeors give us the opportunity to test the observation-based (Jiang et al. 2011, AS13) analyses of characteristics of clouds and precipitation associated with the northward propagating BSISOs. Therefore, in the present study our objective is to use the revised version of CFSv2 to test the hypothesis put forward by the above papers and evaluate the structure and evolution of the dynamical fields, cloud hydrometeors and the large-scale heating components during the northward propagating BSISOs. Data, model description and methodology are given in Sect. 2. Results and discussions are given in Sect. 3 and Sect. 4 summarizes and concludes the study.

2 Data, model description, and methodology

The latest version of NCEP CFSv2 (Saha et al. 2014) is a fully coupled ocean-land-atmosphere dynamical modeling system. It comprises of NCEP Global Forecast System (GFS) atmospheric GCM (Moorthi et al. 2001) and Geophysical Fluid Dynamics Laboratory (GFDL) Modular Ocean Model version 4p0d (Griffies et al. 2004) as oceanic component. The atmospheric component has a spectral resolution of T126 (~ 100 km) with 64 sigma-pressure hybrid vertical layers and the oceanic component has zonal resolution of 0.25°–0.5° with 40 vertical layers. More details about the CFSv2 model and its various physical schemes are well documented in Saha et al. 2014. The revised version of CFSv2 includes RSAS convective parameterization scheme (Han and Pan 2011). The detailed descriptions about RSAS are well documented in Han and Pan (2011). The model also uses simple cloud microphysics scheme with

ice physics developed by Zhao and Carr (1997) based on Sundqvist et al. (1989). In addition to RSAS scheme, a six-class WSM6 microphysics scheme (Hong and Lim 2006) is incorporated in place of two-class Zhao and Carr (1997) microphysics scheme in CFSv2. Prognostic water substance variables in WSM6 contain water vapour, cloud water, cloud ice, rain water, snow and graupel. More detailed description about WSM6 can be found in Hong and Lim (2006). In order to keep consistency with the modified convective and cloud microphysical processes, the cloud hydrometeors generated by WSM6 are included during the computation of cloud fraction in RRTM radiation scheme. Further details about the model set up are documented in Abhik et al. (2017). It is worth to mention that in WSM, the individual cloud hydrometeors are computed explicitly based on tendency equations (Hong et al. 2004; Hong and Lim 2006) associated with each cloud hydrometeor species while in the ZC scheme, the prognostic equation considers cloud condensate (consisting of CLW and CLI) as the predictive variable (Eq. 3 of Zhao and Carr 1997) and the individual hydrometeors (CLW and CLI) are estimated diagnostically following Zhao and Carr 1997. We have carried out two separate free runs of 15 years of CFSv2 with RSAS and default microphysics scheme (Zhao and Carr; ZC hereafter) and with RSAS and WSM6 scheme with the same initial condition. Both atmospheric and oceanic initial conditions are taken from NCEP Climate Forecast System Reanalysis (CFSR; Saha et al. 2010). For better readability, CFSv2 with RSAS (RSAS) and ZC (WSM6) microphysics scheme is referred as RSAS-ZC (RSAS-WSM) throughout the manuscript. Here by free run, we mean that the models RSAS-ZC and RSAS-WSM are being integrated continuously without any updates and this approach is helpful in diagnosing model's systematic bias.

To validate the model simulation, various observational and reanalyses data sets are used. The Tropical Rainfall Measuring Mission (TRMM) 3B42 version 7 (V7) (Huffman et al. 2007) daily data at a horizontal resolution of $0.25^\circ \times 0.25^\circ$ for the year 1999–2012 are used in the present study. In order to identify the strong and weak events, we have adopted similar methodology based on the study by AS13. We have applied a 20–90 day band-pass Lanczos filter (Duchon 1979) to the daily rainfall anomalies for both the observation and the model data. The choice of the frequency band (20–90 days) is based on the power spectrum analyses for both the observation and model simulated rainfall (Figure not shown). The daily rainfall anomalies are calculated by removing the annual cycle (defined by mean and first three harmonics) from the daily rainfall data. A precipitation index (PI) is defined for each year from 1 June to 30 September by using filtered precipitation anomalies averaged over the box (74°E – 85°E , 18°N – 27°N) representing the core ISM domain (Ganai et al. 2016). The normalization of precipitation index

is done by dividing the time series by its own standard deviation. The identification of strong and weak events is done based on the value of normalized index. If the normalized index is greater (less) than 1.5 ($0.4 < \text{PI} < 1.0$) for consecutive 3 days or more, it is considered as strong (weak) BSISO period (Fig. 1). The above methodology is applied for both the observation and model data in order to identify strong and weak cases. The “lag0” composite and convection center is defined similar to AS13. The identification of “lag0” day is marked as the day on which the PI value becomes maximum for a particular northward propagating event.

3 Results and discussions

3.1 Northward propagation of rainfall

To begin the analyses, we construct the lag composite of filtered precipitation anomaly from TRMM and simulations of both the model during strong and weak BSISO cases (defined in Sect. 2). This will bring out the model's fidelity to capture the characteristics of large-scale organization of precipitation during the strong and weak BSISO events. Based on TRMM 3B42 rainfall data, the positive (negative) rainfall anomalies are found to be situated over the EIO (Bay of Bengal) and over the southern Indian peninsular (northern Indian) region at “lag –10” during the strong BSISO events (Fig. 2a). Further, the positive rainfall anomalies intensify and propagate northward and establish an extended northwest-southeast tilted rain band structure at “lag 0” over the monsoon trough region. During this phase, the central Indian region experiences an enhanced rainfall activity which corresponds to the active (wet) phase of ISM. At the same time (lag 0), notable negative rainfall anomalies appear

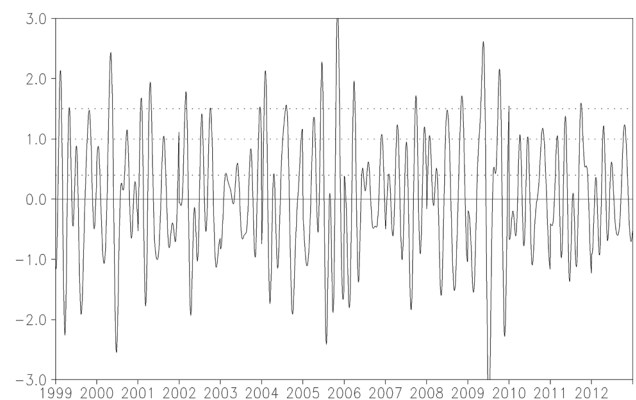
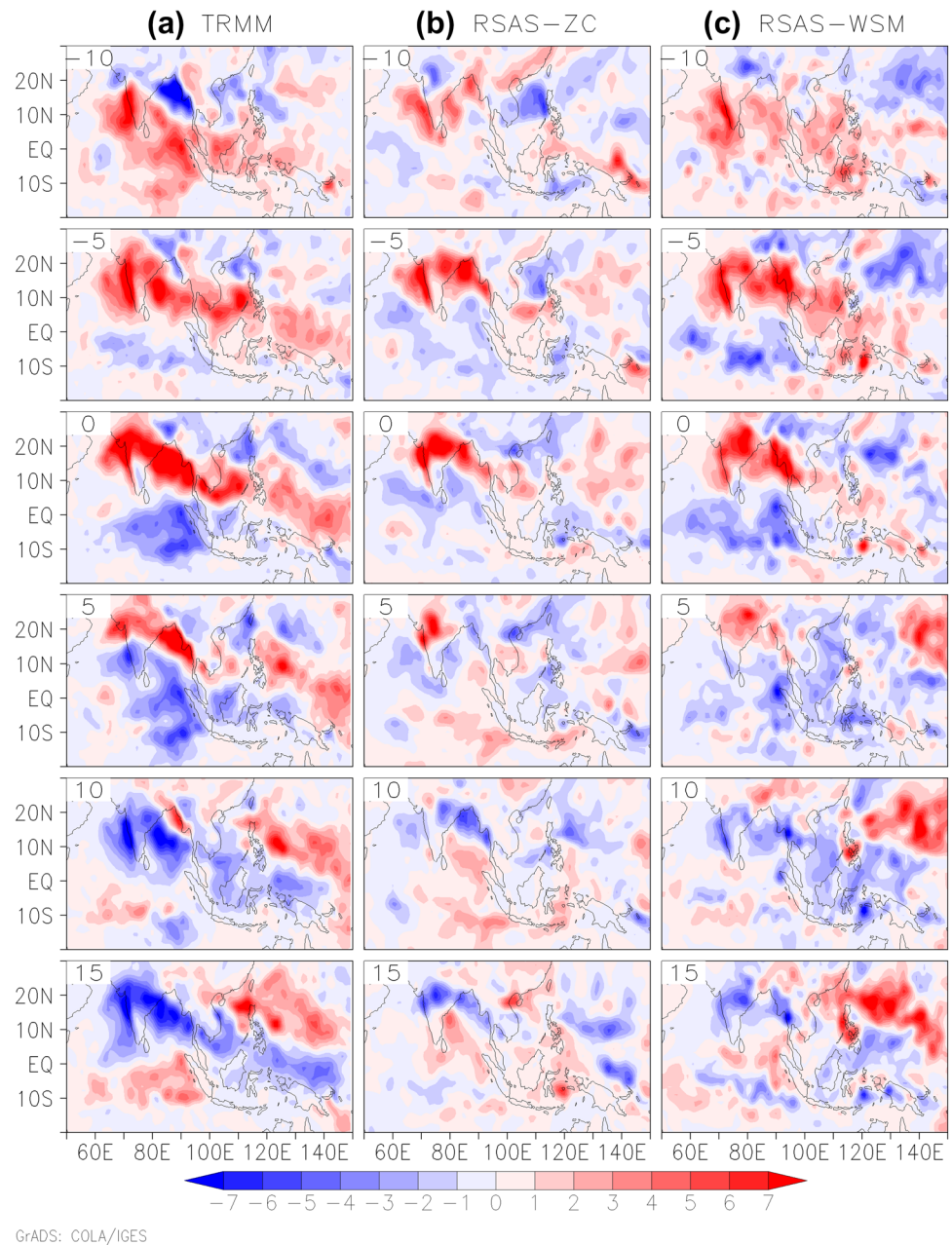


Fig. 1 Time series of 20–90 days filtered precipitation anomalies averaged over CI (18°N – 27°N , 74°E – 85°E) for JJAS from 1999 to 2012 using TRMM 3B42 data sets, normalized by its own standard deviation. Strong (weak) events correspond to the index $> +1.5$ ($0.4 < \text{PI} < 1.0$)

Fig. 2 Lag composite of precipitation anomaly (mm day^{-1}) for strong BSISO events from **a** TRMM, **b** CFSv2 with RSAS-ZC and **c** RSAS-WSM simulation. Lag “days” are noted in the top left corner in each panel



over the EIO region which further intensifies and progresses northward and situates over the monsoon trough region at “lag + 15” (Fig. 2a). This situation corresponds to a reduced rainfall activity over the Indian land mass region and known as the break (dry) phase of ISM. Similar features related to the northward propagation of BSISOs has also been reported by many previous studies (Jiang et al. 2004, 2011; Goswami 2005; Halder et al. 2012, AS13) based on the observations. It is worth to see whether the models are able to simulate the observed features of BSISOs during strong events. Both the models are able to capture the northward propagation of rainfall during strong monsoon BSISOs as depicted in Fig. 2b, c respectively. However, closer analyses reveal

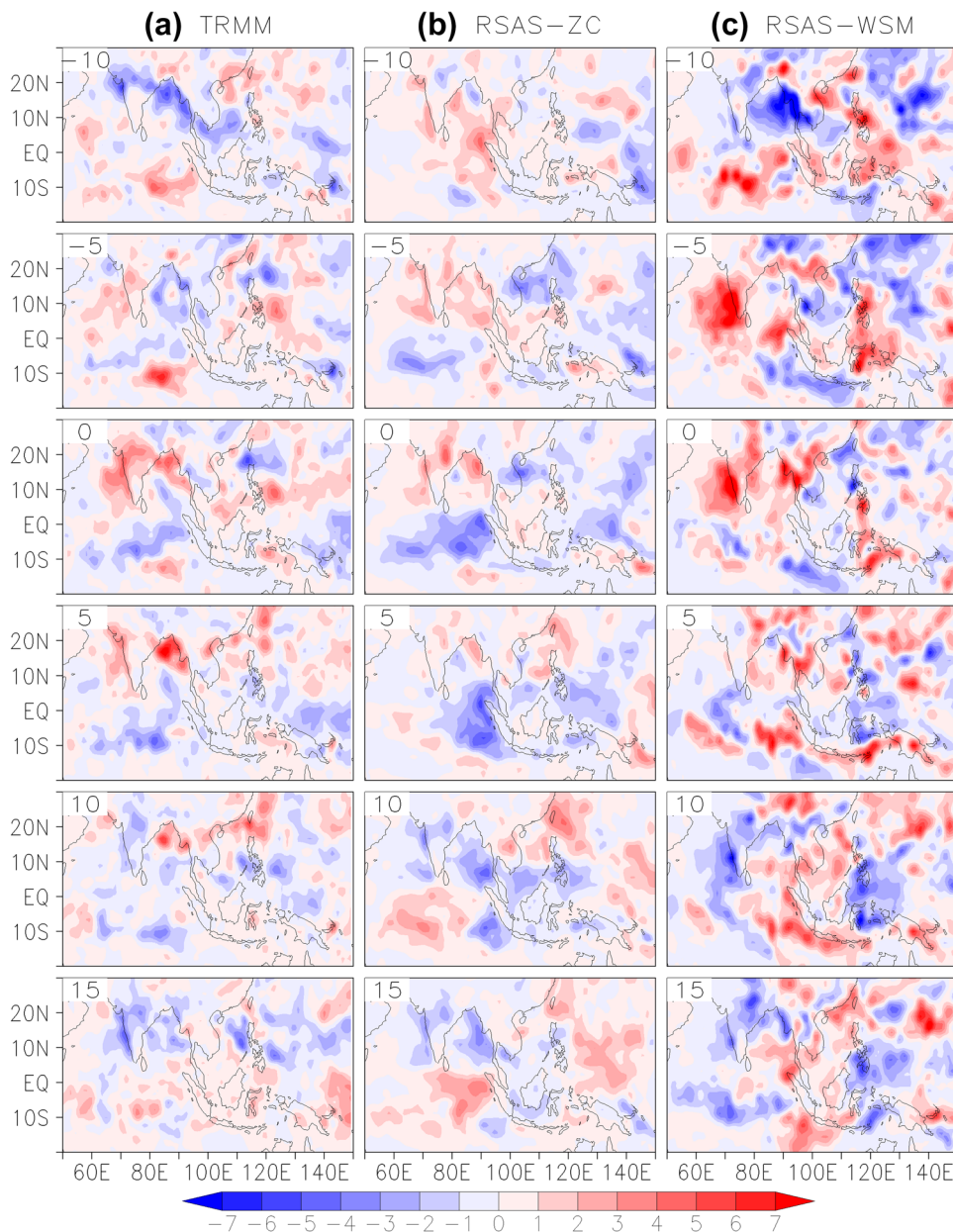
that the CFSv2 with RSAS-ZC scheme poorly simulates the large-scale organized rain band and its tilted structure for all the lags (Fig. 2b) as compared to the observation. Additionally, the formation of prominent suppressed rainfall activity over the EIO region is weak in RSAS-ZC scheme particularly in “lag - 5” and “lag 0”. On the other hand, CFSv2 with RSAS-WSM simulation (Fig. 2c) shows an improved northward propagating BSISO features during the strong events. The large-scale organized rainfall structure with a tilt in north-west to south-east direction is particularly evident in “lag - 10”, “lag - 5” and “lag 0” (Fig. 2c). In “lag - 10” (Fig. 2c) the RSAS-WSM shows a positive rainfall anomaly over the southern peninsular India extending

up to Maritime continents which is much realistic when compared to TRMM (Fig. 2a). Positive rainfall anomaly in subsequent lags (“lag - 5” and “lag 0”) moved to the north with enhanced intensity and with the tilt being maintained (Fig. 2c). Due to better large-scale organization of rainfall band, RSAS-WSM shows noticeable improvement in rainfall propagation over the West Pacific region as compared to the observation (Fig. 2a).

During the weak BSISOs, reduced rainfall activity with less prominent northward propagation is evident both in the observation (Fig. 3a) and model (Fig. 3b, c) simulations. The extended large-scale organization of the positive rainfall anomaly and its associated tilt (north-west to south-east) in

rain band are missing during weak composites. TRMM rainfall anomaly during weak BSISOs, shows (Fig. 3a) a positive anomaly of rainfall at Lag 0 with much reduced magnitude. Although RSAS-ZC simulation shows a comparable magnitude of rainfall as that of TRMM (Fig. 3b), RSAS-WSM overestimates the rainfall amplitude during the weak BSISO events as compared to TRMM (Fig. 3c) particularly over the west coast region of India in “lag - 5” and “lag 0”. To examine the propagation features of BSISOs over the Indian land mass region, we have analyzed the lag-latitude plot of rainfall anomaly averaged over 70°E–90°E during the strong and weak events (Fig. 4). During the strong BSISOs, TRMM shows (Fig. 4a) a well-organized positive rainfall anomaly

Fig. 3 Lag composite of precipitation anomaly (mm day^{-1}) for weak BSISO events from **a** TRMM, **b** CFSv2 with RSAS-ZC and **c** RSAS-WSM simulation. Lag “days” are noted in the top left corner in each panel



GrADS: COLA/IGES

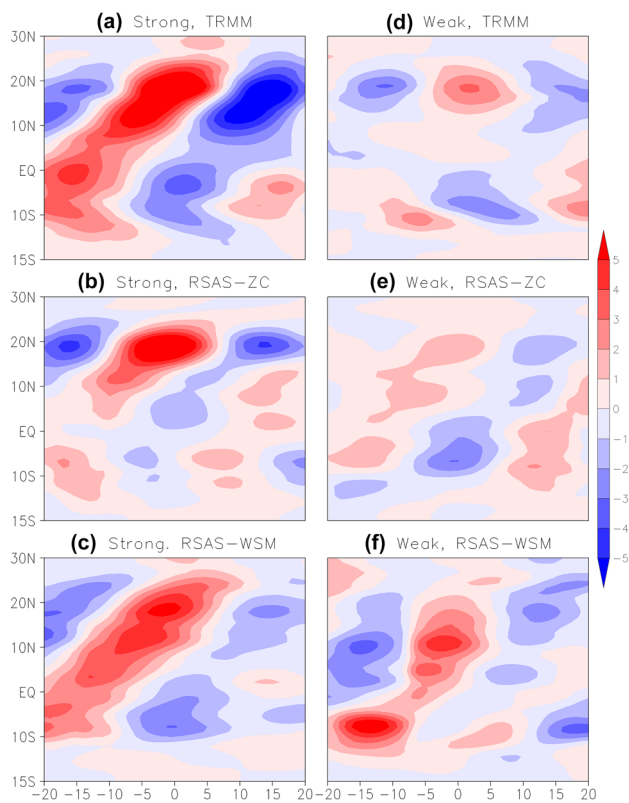


Fig. 4 Lag-Latitude Hovmöller plot of filtered precipitation anomaly (mm day^{-1}) averaged over 70°E – 90°E for strong BSISO cases from a TRMM, CFSv2 with b RSAS-ZC and c RSAS-WSM scheme respectively. d–f Represents similar analyses but for weak BSISO events

propagating northward from the EIO to 25°N followed by a negative rainfall anomaly. CFSv2 with RSAS-ZC scheme shows a weak northward propagating positive anomaly of rainfall as compared to the TRMM (Fig. 4b) instead it shows a stationary pattern of positive rainfall anomaly confined over the Indian landmass. RSAS-WSM scheme is able to better reproduce the northward propagation of BSISOs (Fig. 4c) for the strong BSISOs. However, slight underestimation of magnitude of rainfall anomaly is noted in Fig. 4c. During the weak events, the northward propagation of BSISOs is less prominent with reduced magnitude both in the observation (TRMM) and in the model simulations (Fig. 4d–f) although RSAS-WSM has an overestimation of rainfall over the EIO and around 10°N as seen in the spatial plot (Fig. 3c).

The above analyses indicate that RSAS-WSM shows a better fidelity in capturing the large-scale organized structure (e.g. spatial distribution, northwest–southeast tilt) of total rainfall during the northward propagation of strong BSISOs. Earlier studies (Fu and Wang 2004; Chattopadhyay et al. 2009; Halder et al. 2012) showed that the ISM rainfall consists of two major components, namely the convective and stratiform rainfall, and it is the large-scale or stratiform rainfall that plays an important role in the northward propagation

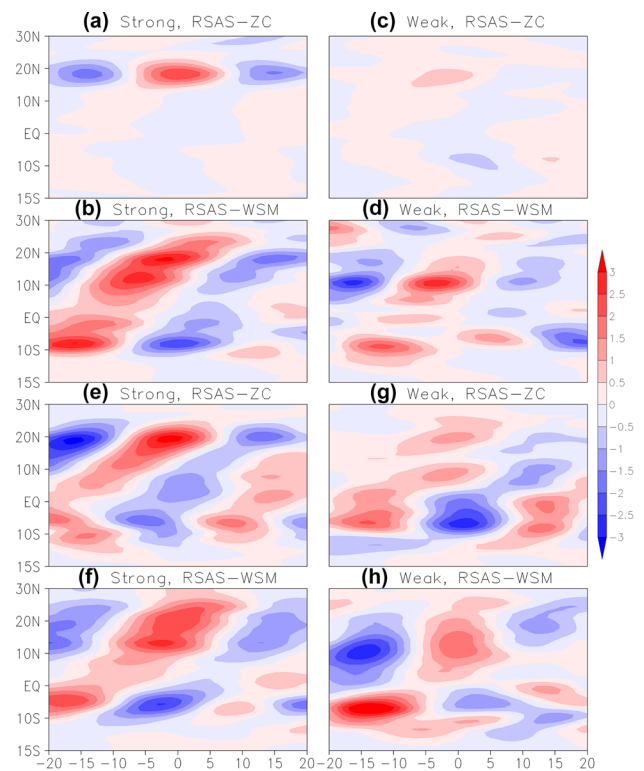


Fig. 5 Lag-Latitude Hovmöller plot of filtered large-scale rainfall anomaly (mm day^{-1}) averaged over 70°E – 90°E for strong BSISO cases from CFSv2 with a RSAS-ZC and b RSAS-WSM scheme. Similar analyses but for weak BSISO events plotted for CFSv2 with c RSAS-ZC and d RSAS-WSM scheme. e–h Represents similar analyses but for convective rainfall during strong and weak BSISO events respectively

of positive rainfall (convective and stratiform) anomaly. Hence, it will be interesting to see whether both the models are able to simulate the northward propagation of convective and stratiform (large-scale) rainfall. It is worth to mention that the criteria for separating the convective and stratiform (large-scale) rainfall are different in the TRMM observation and in the model. In the model, the rainfall from convective parameterization is considered to be convective rainfall and that from the grid-scale microphysics process is considered as the large-scale (stratiform) rainfall (Ganai et al. 2016; Abhik et al. 2017). In the present study, we are comparing convective and large-scale rainfall between the two model simulations (Fig. 5). By using TRMM-3G68 data, Chattopadhyay et al. (2009) showed (Fig. 8 in their paper) that the stratiform rainfall exhibits a well-defined large-scale organized structure with steady northward propagation associated with the active phases of ISOs. CFSv2 with RSAS-ZC fails to show northward propagation of large-scale rainfall during the strong BSISO events (Fig. 5a). It also shows a localized heavy large-scale rainfall over the central Indian region ($\sim 20^{\circ}\text{N}$) at “lag 0” consistent with the plot of total rainfall

(Fig. 4b). Additionally, the contribution from the large-scale rainfall is considerably less for all the lags as compared to RSAS-WSM (Fig. 5b). The large-scale rainfall distribution shows considerable improvement in RSAS-WSM simulation as depicted in Fig. 5b. It is able to capture the large-scale (10°S – 25°N) organized structure to a reasonable extent and northward progression of the large-scale rainfall is clearly evident and consistent with the lag composite of the spatial distribution of stratiform rainfall for various lags (Figure not shown). Earlier studies (Chattopadhyay et al. 2009; Halder et al. 2012) suggested that the convective component of the total rain does not show pronounced northward propagation associated with strong BSISOs. However, both the models appear to show a reasonable northward propagation of convective rainfall during strong BSISO events (Fig. 5c, d). During weak BSISOs, the lack of organization of large-scale rainfall and convective rainfall is apparent (Fig. 5c, d, g, h) in both the models. However, marginal northward propagation is noted in Fig. 5d, g.

3.2 Northward propagation of cloud hydrometeors and large-scale condensation heating

Earlier studies (Jiang et al. 2011; Halder et al. 2012 and AS13) demonstrated the importance of cloud hydrometeors on the northward propagation of BSISOs. In this section, we would discuss the model fidelity in capturing the distribution of cloud hydrometeors during the strong and weak BSISOs. As we have noted that RSAS-WSM simulation better reproduces the northward propagating BSISOs (Fig. 4c) compared to RSAS-ZC simulation, it will be worth to evaluate the model performance in capturing different cloud hydrometeors associated with the BSISOs. The lag composite of anomalous cloud liquid water (CLW, shaded) and cloud ice (CLI, red contour) averaged over 70°E – 90°E along with the anomalous rainfall (bottom panel) is shown for both the model versions in Fig. 6a, b respectively for the strong BSISO events. By using TRMM data, AS13 showed (Fig. 5 in their paper) that anomalous CLW and CLI exhibits a steady northward progression along with the positive rainfall anomaly associated with the strong BSISOs. CFSv2 with RSAS-ZC scheme fails to simulate a coherent northward propagation of CLW and CLI at various lags (Fig. 6a) along with the rainfall. At “lag – 10” (Fig. 6a) positive rainfall anomaly is seen to be around 10°N but the CLW does not show any positive anomaly although CLI shows a positive anomaly at the upper level. In the subsequent “lag – 5”, the rainfall moves northward and the CLI also shows a northward movement while CLW still shows a negative anomaly at the lower level. On “lag 0”, however, the model (RSAS-ZC) simulates a positive CLW anomaly collocated with the positive rainfall anomaly and a positive CLI anomaly slightly to the south in the upper level. The propagation

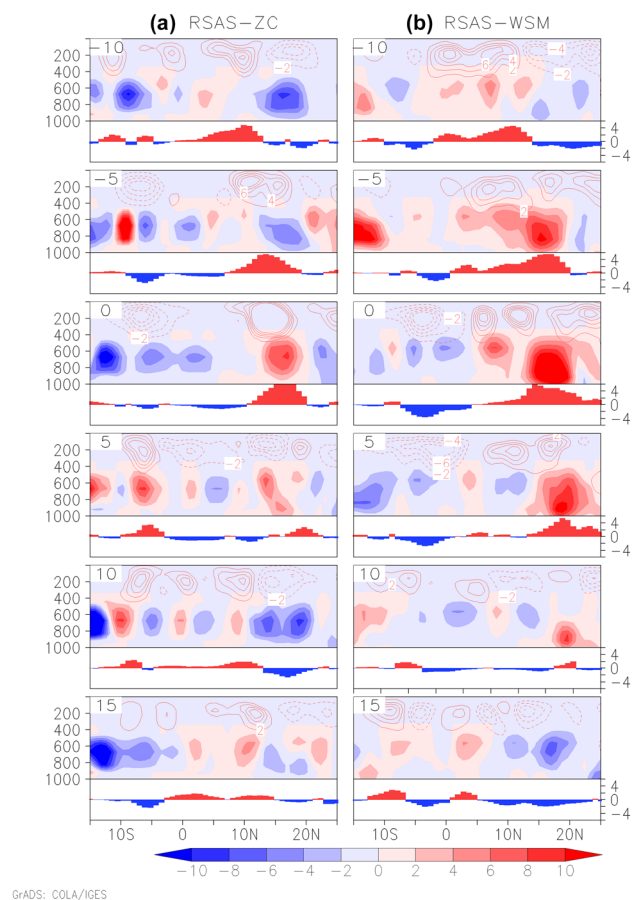


Fig. 6 Time evolution of pressure-latitude profiles (upper part in each panel) of anomalous CLW ($\times 10^{-6} \text{ kg kg}^{-1}$, shaded) and CLI ($\times 10^{-6} \text{ kg kg}^{-1}$, red contour, solid (dashed) represents positive (negative) anomaly) over 70°E – 90°E during strong BSISO cases from CFSv2 with **a** RSAS-ZC and **b** RSAS-WSM simulations. At lower part in each panel corresponding rainfall anomaly (mm day^{-1}) over the same region is shown. The red (blue) shading denotes enhanced (reduced) rainfall activity

of rain and the hydrometeors are not evident beyond “lag 0” in RSAS-ZC simulation. On the contrary, RSAS-WSM (Fig. 6b) shows a more realistic northward propagation of CLW, CLI and the rainfall as showed earlier based on observation by AS13 and Jiang et al. (2011). It is evident from Fig. 6b, that a positive rainfall anomaly evolving around the equator along with a positive anomaly of CLW and CLI, moves steadily northward reaching up to 25°N by “lag + 5” and dissipating subsequently (“lag + 10”) and reappearing over the oceanic region around 10°S at “lag + 15”. The above analyses, evidently shows a better fidelity of RSAS-WSM in reproducing the observation-based relation of cloud hydrometeors and rainfall associated with the northward propagation of BSISOs.

The CLW and CLI play an important role in terms of heating distribution in the atmospheric column which in turn influences the atmospheric divergence and convergence

through convective coupled feedback (AS13). It is likely that improved representation of cloud microphysical processes in WSM scheme helps in simulating a better CLW and CLI distribution associated with the strong BSISOs as compared to ZC scheme in CFSv2. In contrast to the northward propagation of BSISOs during the strong events, the weak composites of anomalous CLW and CLI do not show prominent northward propagation (Figure not shown) in both the models.

The importance of CLW and CLI on the modulation of large-scale heating distribution has been echoed by several studies (Baker 1997, AS13). As the large-scale cloud hydrometeors distribution is improved in RSAS-WSM simulation during the strong BSISO events, it is worth to look into the large-scale heating structure during the northward propagation of BSISOs. AS13 demonstrated that the large-scale heating distribution showed a quasi-periodic propagation associated with the northward progression of BSISOs. Figures 7 and 8 demonstrate the large-scale condensation heating profile for various lags associated with the strong BSISO events from RSAS-ZC and RSAS-WSM simulations respectively. CFSv2 with RSAS-ZC simulation does not show any prominent northward propagation of large-scale condensation heating and it is consistently weaker for all the lags except for “lag 0” over 20°N–25°N (Fig. 7). In contrast, RSAS-WSM scheme is able to simulate the quasi-periodic northward propagation of large-scale heating to a reasonable extent (Fig. 8). For “lag -10” to “lag 5”, the mid-level heating is followed by low-level cooling which indicates the baroclinic nature of the monsoon ISOs (Fig. 8). Drbohlav

and Wang (2005) demonstrated from 2D model experiment that the baroclinic mode plays an important role in enhancing the intensity of the convection through upper level divergence and lower level convergence leading to more moisture into the convection centre. Such kind of distribution is missing in RSAS-ZC simulation (Fig. 7). It is likely that the realistic simulation of grid scale cloud hydrometeors appear to have led to a reasonable large-scale heating distribution in RSAS-WSM simulation which further helps in capturing realistic northward propagation of rainfall.

3.3 Dynamical and thermodynamical response associated with the BSISO

From the above analyses, it is evident that RSAS-WSM scheme shows a better northward propagation of the large-scale organized structure of rainfall, cloud hydrometeors and large-scale heating structure as compared to RSAS-ZC scheme in CFSv2. However, the dynamical and thermodynamical processes associated with the northward progression of BSISOs need to be investigated which will further test the theory proposed by AS13 regarding northward propagation of BSISOs in both the models. In view of the above, the vertical profiles of various dynamical and thermodynamical parameters associated with the BSISOs are examined with respect to the maximum convection center for both the models. Earlier studies (Jiang et al. 2004; Halder et al. 2012, AS13) mentioned that a barotropic vorticity lies to the north of the MCC (Fig. 6a of AS13) during strong BSISO events. Although both the models are able to capture the barotropic

Fig. 7 Lag composite of CFSv2 with RSAS-ZC scheme simulated large-scale condensation heating anomaly (Kday^{-1}) for strong BSISO events. Lag “days” are noted in the top left corner

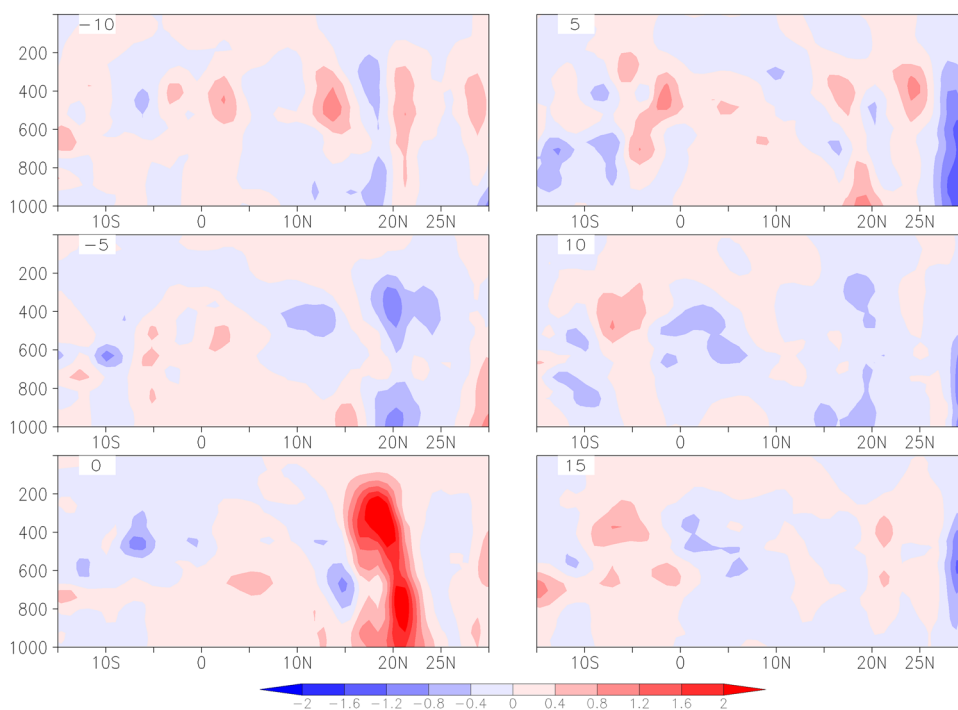
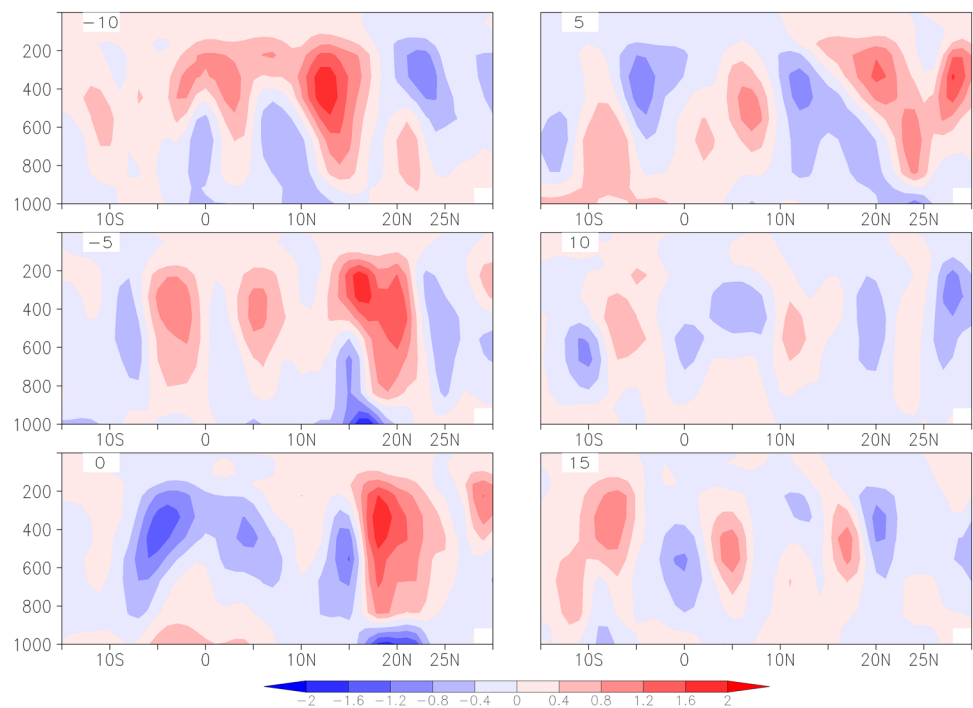


Fig. 8 Lag composite of CFSv2 with RSAS-WSM scheme simulated large-scale condensation heating anomaly (Kday^{-1}) for strong BSISO events. Lag “days” are noted in the top left corner



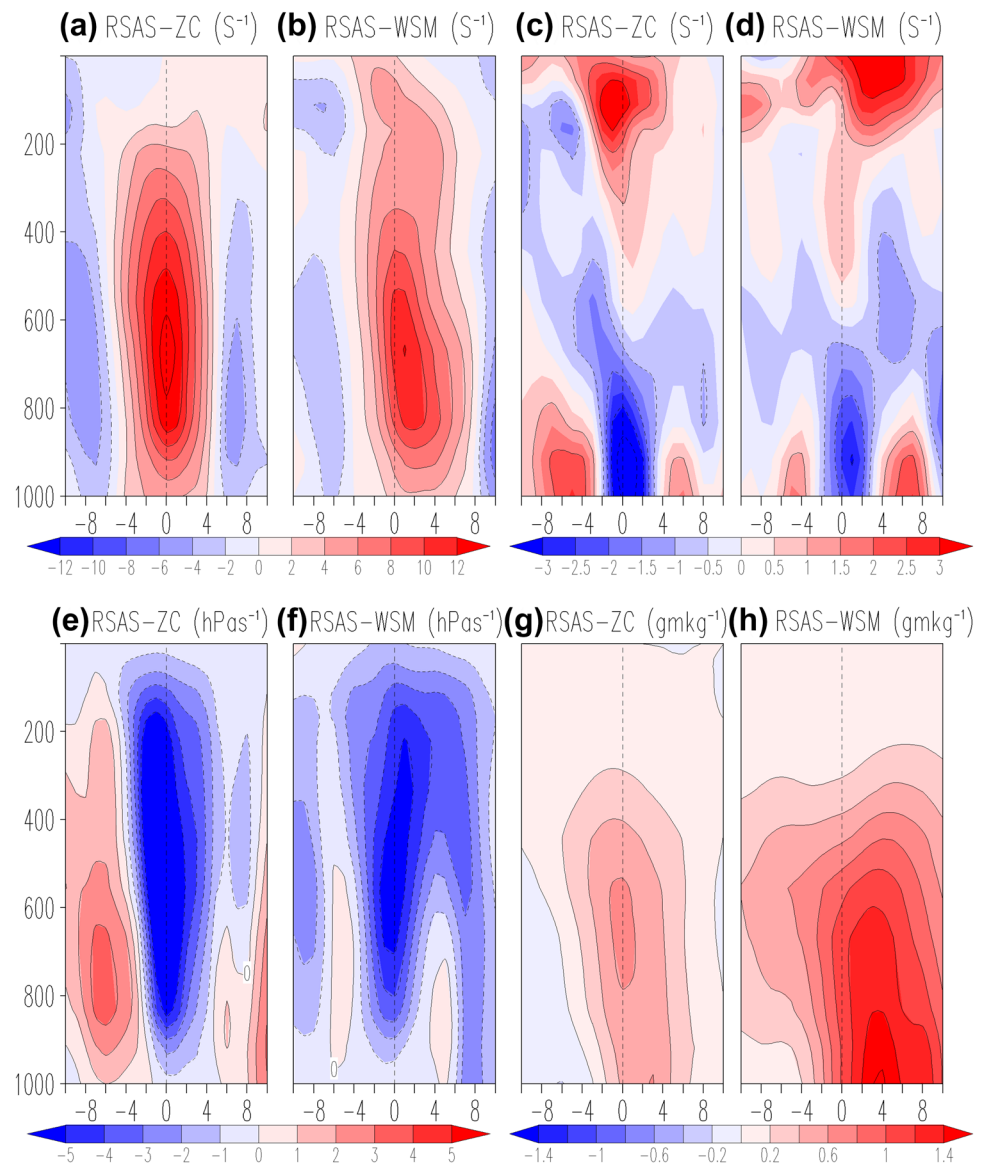
nature of the vorticity (Fig. 9a, b), in RSAS-ZC simulation, it is collocated with the MCC (Fig. 9a). On the contrary, in RSAS-WSM it is slightly to the north of the MCC (Fig. 9b).

The anomalous low level convergence is found to be nearly collocated with the MCC in RSAS-ZC (Fig. 9c) whereas it is to the north of the convection center in RSAS-WSM simulation (Fig. 9d) which is consistent with the observation-based analyses (Fig. 6b of AS13). Studies by Jiang et al. (2004) and AS13 have suggested that the asymmetric distribution of these dynamical parameters with respect to the MCC plays a key role in the northward propagation of BSISOs. The RSAS-ZC scheme fails to capture such observed relationship of dynamical parameters which is consistent with the model’s poor ability to simulate northward propagation. On the contrary, RSAS-WSM with improved representation of cloud hydrometeors and the dynamical properties is able to show a realistic relationship of rainfall and hydrometeors in terms of northward propagation as shown in AS13 and Jiang et al. (2011). The vertical velocity profile shows a barotropic structure in both the models and collocates with the MCC (Fig. 9e, f) which is similar to the observation reported by (Fig. 6c in AS13). Earlier studies (Jiang et al. 2011 and AS13) showed that the low level moistening ahead of the MCC plays a major role in lower level preconditioning and triggering of deep convection to the north of the convection center. To test this process, we have plotted the anomalous specific humidity (Fig. 9) where the RSAS-ZC shows (Fig. 9g) the low level specific humidity maximum at around 700 hPa and also collocated with the convection center. On the other hand,

RSAS-WSM shows the maximum of specific humidity to be located to the north of the convection center and below the 800 hPa (Fig. 9h). Hence, it indicates that the RSAS-ZC (RSAS-WSM) scheme is unable (able) to reproduce the lower tropospheric moist process realistically which is necessary for triggering the convection ahead of the MCC. It is likely to be one of the main reasons for lack (proper) of organized large-scale northward propagation of rainfall and cloud hydrometeors distribution in RSAS-ZC (RSAS-WSM) simulation. Similar improvement of lower tropospheric moistening in CFSv2 with RSAS-WSM was shown by Abhik et al. (2017) over the ISM domain during summer monsoon. Consistent with the location of barotropic vorticity and lower level convergence within the planetary boundary layer, the moisture convergence in RSAS-ZC is found to be nearly collocated with the MCC (Fig. 10a) unlike the RSAS-WSM where it is found slightly to the north of the MCC (Fig. 10b). We have also analyzed the vertical structure of CLW and CLI with respect to the MCC for both the models (Fig. 10c, d) during the strong BSISOs. Jiang et al. (2011), Halder et al. (2012) and AS13 showed that the CLW (CLI) maximum appears to the north (south) of the MCC (Fig. 8a of AS13). CFSv2 with RSAS-ZC simulates the CLW which is nearly collocated with the MCC (Fig. 10c) while RSAS-WSM scheme shows the CLW maximum slightly to the north of the MCC (Fig. 10d). The magnitude of the CLW is much higher in RSAS-WSM as compared to RSAS-ZC scheme.

In order to look into the model fidelity in capturing the dynamical and thermodynamical processes during weak

Fig. 9 Meridional-vertical structures of **a, b** vorticity ($\times 10^{-6} \text{ s}^{-1}$), **c, d** divergence ($\times 10^{-6} \text{ s}^{-1}$), **e, f** vertical velocity (hPa s^{-1}) and **g, h** specific humidity (g kg^{-1}) from RSAS-ZC and RSAS-WSM simulation respectively during strong BSISO cases. X-axis represents the meridional distance (degree) with respect to the maximum convection center (represented in vertical black line). The +ve (−ve) value suggests north (south) of the maximum convection center. Y-axis represents pressure levels in hPa



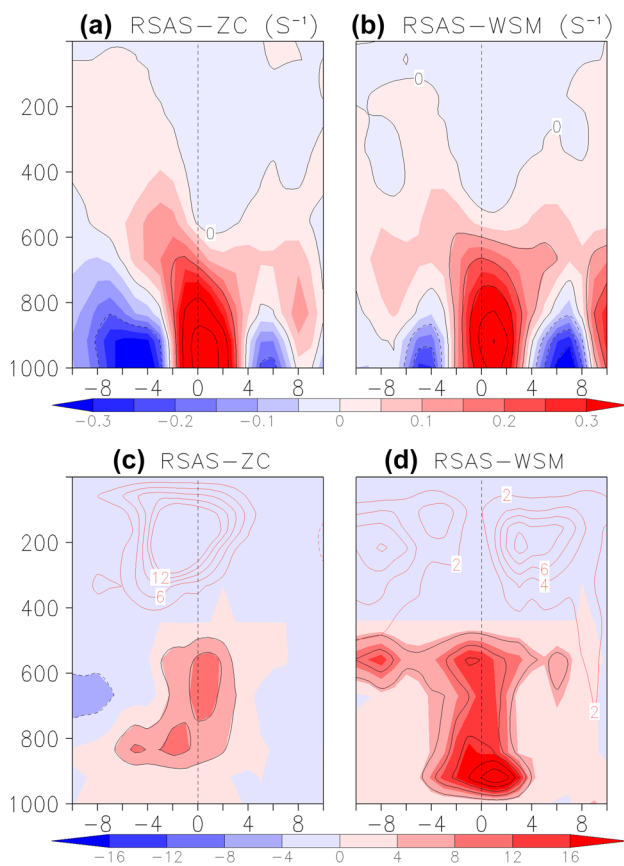
GRADS: COLA/IGES

BSISO events, we have analyzed few parameters in Fig. 11. It is noted that the distribution of vorticity and divergence exhibit broadly similar patterns as in the strong BSISO cases but with much weaker magnitude (Fig. 11a–d). These results (of RSAS-WSM) are consistent with the study by AS13 during the weak BSISO cases.

All the above analyses indicate that the CFSv2 with RSAS-WSM shows a better fidelity in capturing all the dynamical and moist processes which has helped in improving the northward propagation of BSISOs as compared to RSAS-ZC simulations. The above analysis also demonstrates that better representation of cloud processes help the RSAS-WSM model to capture the observed dynamical and thermodynamical features of BSISOs.

4 Summary and conclusions

In the present study, a revised version of CFSv2 is used to evaluate its fidelity in capturing the structure and evolution of the dynamical, thermodynamical fields, cloud hydrometeors and the large-scale heating components during the northward propagation of strong and weak BSISOs. The revised version of CFSv2 consists of RSAS convective parameterization scheme and WSM6 cloud microphysics scheme whereas default version of CFSv2 has RSAS convective and ZC cloud microphysics scheme. Abhik et al. (2017) demonstrated the impact of WSM scheme in simulating various aspects of mean and intraseasonal ISM features. They have documented considerable improvement in convective



GrADS: COLA/IGES

Fig. 10 Meridional-vertical structures of **a, b** moisture convergence ($\times 10^{-6} \text{ s}^{-1}$) and **c, d** CLW (shaded and black contoured) and CLI (red contoured) ($\times 10^{-6} \text{ kg kg}^{-1}$) RSAS-ZC and RSAS-WSM simulation respectively during strong BSISO cases. The x-axis and y-axis are same as Fig. 9

and large-scale rainfall and the northward propagation of BSISOs during ISM resulted from realistic representation of grid scale cloud processes in addition to better sub-grid scale convection in CFSv2. Further, this study aims to test the hypothesis proposed by AS13, Jiang et al. 2011 based on the observation which is mentioned in Sect. 1.

The study reveals that CFSv2 with RSAS-ZC finds it difficult to capture the large-scale organization as well as the northwest-southeast tilted structure of rain band as compared to TRMM. Additionally, it reproduces localized enhanced rainfall activity at “lag 0” over the Indian land mass region during the strong BSISO events. On the contrary, CFSv2 with RSAS-WSM scheme simulates the large-scale organization and tilted structure of rainfall reasonably well. Earlier studies (Chattopadhyay et al. 2009; Halder et al. 2012) showed that the large-scale organized northward propagation of total rainfall is mostly dominated by the stratiform component of the total rain whereas the convective component hardly shows any large-scale organization. It is found that

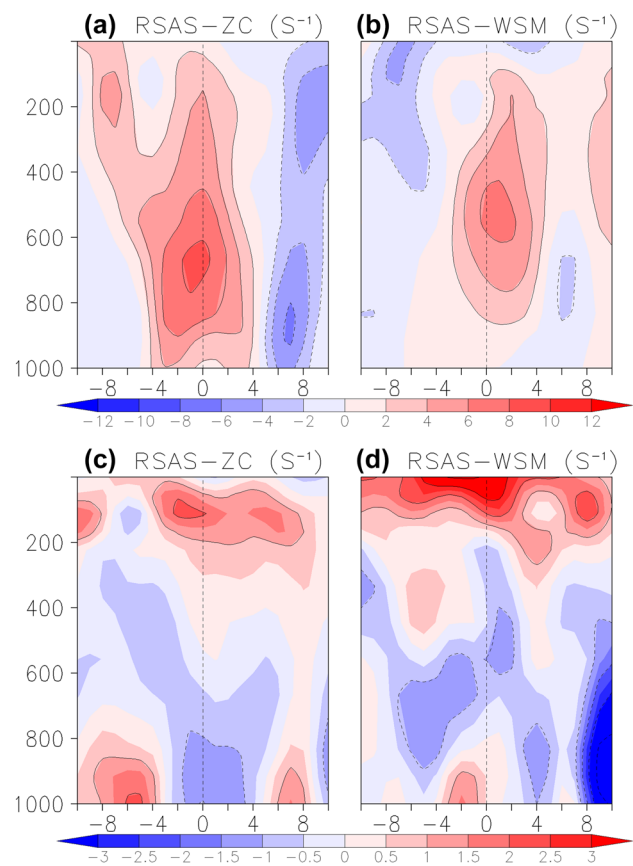


Fig. 11 Meridional-vertical structures of **a, b** vorticity ($\times 10^{-6} \text{ s}^{-1}$) and **c, d** divergence ($\times 10^{-6} \text{ s}^{-1}$) from RSAS-ZC and RSAS-WSM simulation respectively during weak BSISO cases. The x-axis and y-axis are same as Fig. 9

RSAS-WSM shows a much better organization of large-scale rainfall and shows a steady northward propagation during strong BSISO events contrary to RSAS-ZC.

As the cloud microphysical processes are better represented in WSM scheme, we have looked into the northward propagation of different cloud hydrometeors during the strong and weak BSISO cases. The pressure-latitude profiles of anomalous CLW and CLI shows a reasonable steady northward propagation along with rainfall anomaly in RSAS-WSM consistent with the observation (AS13). The realistic simulation of CLW and CLI modulates the heating distribution in the atmospheric column which further influences the divergence and convergence in a convectively coupled monsoon system (Jiang et al. 2011). It is further established from the pressure-latitude profiles of anomalous large-scale condensation heating distribution. It is seen that the RSAS-WSM simulates a reasonable quasi-periodic northward propagation of large-scale heating consistent with the large-scale cloud hydrometeors distribution. In contrast, the RSAS-ZC scheme fails to show northward propagation of large-scale heating instead shows a localized heating

profile at “lag 0”. Hence, it appears that the realistic simulation of CLI and CLW in RSAS-WSM leads to the improvement in the large-scale heating distribution consistent with the earlier studies (Jiang et al. 2011, AS13).

The anomalous barotropic vorticity and low level convergence are found to lie to the north of the MCC in RSAS-WSM scheme consistent with the observation-based studies. Another major deficiency in RSAS-ZC is lesser specific humidity in the lower level and the specific humidity being collocated with the MCC. Observation shows specific humidity maximum in the lower troposphere and to the north of the MCC (AS13) which is aptly simulated by the RSAS-WSM. The present study brings out the better fidelity in CFSv2 with RSAS-WSM scheme in simulating the structure, evolution of the dynamical parameters, cloud hydrometeors and large-scale heating profiles associated to the northward propagation of strong BSISOs as proposed by the observation-based studies. The present version (RSAS-WSM) would be tested in hindcast mode to evaluate its potential in improving the forecast skill. This study shows that the hypothesis and relation established based on observation are robust and pave the way for model development and finally model improvement.

Acknowledgements IITM, Pune is fully funded by the Ministry of Earth Sciences (MoES), Government of India, New Delhi. Authors are grateful to the anonymous reviewers and editor for their constructive comments which have helped to improve the manuscript. We would like to thank NASA for providing TRMM data sets. All model runs are carried out on MoES “Aditya” High Performance Computing (HPC) system at IITM, Pune, India. The model simulation is archived at “Aditya” HPC and available on request from the corresponding author.

References

- Abhik S, Halder M, Mukhopadhyay P, Jiang X, Goswami BN (2013) Possible new mechanism for northward propagation of boreal summer intraseasonal oscillations based on TRMM and MERRA reanalysis. *Clim Dyn* 40:1611–1624. <https://doi.org/10.1007/s00382-012-1425-x>
- Abhik S, Krishna RPM, Mahakur M, Ganai M, Mukhopadhyay P, Dudhia J (2017) Revised cloud processes to improve the mean and intraseasonal variability of Indian summer monsoon in climate forecast system: part 1. *J Adv Model Earth Syst* 9:1–28. <https://doi.org/10.1002/2016MS000819>
- Baker MB (1997) Cloud microphysics and climate. *Science* 276:1072–1078
- Chattopadhyay R, Goswami BN, Sahai AK, Fraedrich K (2009) Role of stratiform rainfall in modifying the northward propagation of monsoon intra-seasonal oscillation. *J Geophys Res* 114:D19114. <https://doi.org/10.1029/2009JD011869>
- Chen YH, Del Genio AD (2009) Evolution of tropical cloud regimes in observations and a general circulation model. *Clim Dyn* 32:355–369. <https://doi.org/10.1007/S00382-008-0386-6>
- Duchon CE (1979) Lanczos filtering in one and two dimensions. *J Appl Meteorol* 18:1016–1022
- Fu X, Wang B (2004) The boreal summer intraseasonal oscillations simulated in a hybrid coupled atmosphere-ocean model. *Mon Weather Rev* 132:2628–2649. <https://doi.org/10.1175/MWR2811.1>
- Fu X, Wang B, Li T, McCreary JP (2003) Coupling between northward-propagating, intraseasonal oscillations and sea surface temperature in the Indian Ocean. *J Atmos Sci* 60:1733–1753
- Fu X, Wang B, Tao L (2006) Satellite data reveal the 3-D moisture structure of tropical intraseasonal oscillation and its coupling with underlying ocean. *Geophys Res Lett* 33:L03705. <https://doi.org/10.1029/2005GL025074>
- Ganai M, Mukhopadhyay P, Phani RMK, Mahakur M (2015) Impact of revised simplified Arakawa-Schubert convection parameterization scheme in CFSv2 on the simulation of the Indian summer monsoon. *Clim Dyn* 45:881–902. <https://doi.org/10.1007/s00382-014-2320-4>
- Ganai M, Krishna RPM, Mukhopadhyay P, Mahakur M (2016) The impact of revised simplified Arakawa-Schubert scheme on the simulation of mean and diurnal variability associated with active and break phases of Indian Summer Monsoon using CFSv2. *J Geophys Res Atmos* 121:9301–9323. <https://doi.org/10.1002/2016JD025393>
- Goswami BN (2005) South Asian summer monsoon. In: Lau WK-M, Waliser DE (eds) *Intraseasonal variability of the atmosphere ocean climate system*. Springer, Berlin, pp 19–61
- Goswami BN, Xavier PK (2003) Potential predictability and extended range prediction of Indian summer monsoon breaks. *Geophys Res Lett* 30(18):1966. <https://doi.org/10.1029/2003GL017,810,2003>
- Griffies SM, Harrison MJ, Pacanowski RC, Rosati A (2004) A technical guide to MOM4, GFDL ocean group technical report 5, GFDL, pp 337
- Halder M, Mukhopadhyay P, Halder S (2012) Study of the microphysical properties associated with the Monsoon Intraseasonal Oscillation as seen from the TRMM observations. *Ann geophys* 30(6):897–910
- Han J, Pan H-L (2011) Revision of convection and vertical diffusion schemes in the NCEP global forecast system. *Weather Forecast* 26:520–533. <https://doi.org/10.1175/WAF-D-10-05038.1>
- Hong SY, Lim JOJ (2006) The WRF single-moment 6-class microphysics scheme (WSM6). *J Korean Meteorol Soc* 42:129–151
- Hong SY, Dudhia J, Chen SH (2004) A revised approach to ice microphysical processes for bulk parameterization of cloud and precipitation. *Mon Weather Rev* 132: 103–120. [https://doi.org/10.1175/1520-0493\(2004\)132%3C0103:ARATIM%3E2.0.CO;2](https://doi.org/10.1175/1520-0493(2004)132%3C0103:ARATIM%3E2.0.CO;2)
- Hsu HH, Weng CH, Wu CH (2004) Contrasting characteristics between the northward and eastward propagation of the intraseasonal oscillation during the boreal summer. *J Clim* 17:727–743
- Huffman GJ, Adler RF, Bolvin DT, Gu G, Nelkin EJ, Bowman KP, Stocker EF, Wolff DB (2007) The TRMM multi satellite precipitation analysis: quasi-global, multi-year, combined-sensor precipitation estimates at fine scale. *J Hydrometeorol* 8:33–55
- Jakob C, Tselioudis G (2003) Objective identification of cloud regimes in the tropical western Pacific. *Geophys Res Lett* 30:2082. <https://doi.org/10.1029/2003GL018367>
- Jiang X, Li T, Wang B (2004) Structures and mechanisms of the northward propagating boreal summer intraseasonal oscillation. *J Clim* 17:1022–1039
- Jiang X, Waliser DE, Li JL, Woods C (2011) Vertical cloud structures of the boreal summer intraseasonal variability based on CloudSat observations and ERA-interim reanalysis. *Clim Dyn* 36:2219–2232. <https://doi.org/10.1007/s00382-010-0853-8>
- Kemball-Cook S, Wang B (2001) Equatorial waves and air-sea interaction in the boreal summer intraseasonal oscillation. *J Clim* 14:2923–2942
- Lau WKM, Waliser DE (2005) *Intraseasonal variability in the atmosphere-ocean climate system*. Springer, Heidelberg, p 474

- Lawrence DM, Webster PJ (2002) The boreal summer intraseasonal oscillation: relationship between northward and eastward movement of convection. *J Atmos Sci* 59:1593–1606
- Lin JL, Weickman KM, Kiladis GN, Mapes BE, Schubert SD, Suarez MJ, Bacmeister JT, Lee MI (2008) Subseasonal variability associated with Asian summer monsoon simulated by 14 IPCCAR4 coupled GCMs. *J Clim* 21:4541–4567. <https://doi.org/10.1175/2008JCLI1816.1>
- Madden RA, Julian PR (1971) Detection of a 40–50 day oscillation in zonal wind in tropical Pacific. *J Atmos Sci* 28:702–708
- Madden RA, Julian PR (1994) Observations of the 40–50-day tropical oscillation: a review. *Mon Weather Rev* 122:814–837
- Moorthi S, Pan HL, Caplan P (2001) Changes to the 2001 NCEP operational MRF/AVN global analysis/forecast system. *NWS Tech Proc Bull* 484:14
- Rossow WB, Tselioudis G, Polak A, Jakob C (2005) Tropical climate described as a distribution of weather states indicated by distinct mesoscale cloud property mixtures. *Geophys Res Lett* 32:L21812. <https://doi.org/10.1029/2005GL024584>
- Saha S et al (2010) The NCEP climate forecast system reanalysis. *Bull Am Meteorol Soc* 91:1015–1057
- Saha S, Moorthi S, Wu X, Wang J, Nadiga S, Tripp P, Behringer D, Hou Y-T, Chuang H-Y, Iredell M, Ek M, Meng J, Yang R, Pena Mendez M, van den Dool H, Zhang Q, Wang W, Chen M, Becker E (2014) The NCEP climate forecast system version 2. *J Clim*. <https://doi.org/10.1175/JCLI-D-12-00823.1>
- Sharmila S, Pillai SA, Joseph S, Roxy M, Krishna RPM, Chattopadhyay R, Abhilash S, Sahai AK, Goswami BN (2013) Role of ocean-atmosphere interaction on northward propagation of Indian summer monsoon intra-seasonal oscillations (MISO). *Clim Dyn* 41:1651–1669. <https://doi.org/10.1007/s00382-013-1854-1>
- Sikka DR, Gadgil S (1980) On the maximum cloud zone and the ITCZ over Indian, longitudes during the southwest monsoon. *Mon Weather Rev* 108:1840–1853
- Sperber KR, Slingo JM, Annamalai H (2000) Predictability and the relationship between subseasonal and interannual variability during the Asian Summer Monsoon. *Q J Roy Meteorol Soc* 126:2545–2574
- Sundqvist H, Berge E, Kristjansson JE (1989) Condensation and cloud parameterization studies with a mesoscale numerical weather prediction model. *Mon Weather Rev* 117: 1641–1657. [https://doi.org/10.1175/1520-0493\(1989\)117%3C1641:CACPSW%3E2.0.CO;2](https://doi.org/10.1175/1520-0493(1989)117%3C1641:CACPSW%3E2.0.CO;2)
- Tromeur E, Rossow WB (2010) Interaction of tropical deep convection with the large-scale circulation in the MJO. *J Clim* 23:1837–1853
- Waliser DE, Jin K, Kang I-S, Stern WF, Schubert SD, Wu MLC, Lau K-M, Lee M-I, Krishnamurthy V, Kitoh A, Meehl GA, Galin VY, Satyan V, Mandke SK, Wu G, Liu Y, Park C-K (2003) AGCM simulations of intraseasonal variability associated with the Asian summer monsoon. *Clim Dyn* 21:423–446. <https://doi.org/10.1007/s00382-003-0337-1>
- Wang B, Xie X (1997) A model for the boreal summer intraseasonal oscillation. *J Atmos Sci* 54:72–86
- Wang B, Webster PJ, Teng H (2005) Antecedents and self induction of active-break south Asian monsoon unraveled by satellites. *Geo Res Lett* 32:L04704. <https://doi.org/10.1029/2004GL020996>
- Webster PJ (1983) Mechanisms of monsoon low-frequency variability: surface hydrological effects. *J Atmos Sci* 40:2110–2124
- Webster PJ, Hoyos C (2004) Prediction of monsoon rainfall and river discharge on 15–30 day time scales. *Bull Amer Meteorol Soc* 85(11):1745–1765
- Wong S, Fetzer EJ, Tian B, Lambriksen B (2011) The apparent water vapor sinks and heat sources associated with the intraseasonal oscillation of the Indian summer monsoon. *J Clim* 24:4466–4479
- Xavier PK, Marzin C, Goswami BN (2007) An objective definition of the Indian summer monsoon season and a new perspective on the ENSO-monsoon relationship. *Quart J Roy Meteorol Soc* 133:749–764
- Yang B, Fu X, Wang B (2008) Atmosphere-ocean conditions jointly guide convection of the boreal summer intraseasonal oscillation: satellite observations. *J Geophys Res* 113:D11105. <https://doi.org/10.1029/2007JD009276>
- Yasunari T (1979) Cloudiness fluctuation associated with the Northern Hemisphere summer monsoon. *J Meteorol Soc Jpn* 57:227–242
- Zhang CD (2005) Madden-Julian Oscillation. *Rev Geophys* 43:RG2003. <https://doi.org/10.1029/2004RG000158>
- Zhao Q, Carr FH (1997) A prognostic cloud scheme for operational NWP models. *Mon Weather Rev* 125:1931–1953

Publisher's Note Springer Nature remains neutral with regard to jurisdictional claims in published maps and institutional affiliations.